

# Utility of synthetic MRI in predicting pathological complete response of various breast cancer subtypes prior to neoadjuvant chemotherapy

M. Matsuda<sup>a,\*</sup>, N. Fukuyama<sup>a</sup>, T. Matsuda<sup>b</sup>, S. Kikuchi<sup>a</sup>, Y. Shiraishi<sup>a</sup>,  
Y. Takimoto<sup>a</sup>, Y. Kamei<sup>c</sup>, M. Kurata<sup>d,e</sup>, R. Kitazawa<sup>f</sup>, T. Kido<sup>a</sup>

<sup>a</sup> Department of Radiology, Ehime University Graduate School of Medicine, Shitsukawa, Toon, Ehime, 791-0295, Japan

<sup>b</sup> Department of Medical Informatics, Ehime University Graduate School of Medicine, Shitsukawa, Toon, Ehime, 791-0295, Japan

<sup>c</sup> Breast Center, Ehime University Hospital, Shitsukawa, Toon, Ehime, 791-0295, Japan

<sup>d</sup> Department of Pathology, Ehime University Proteo-Science Center, Shitsukawa, Toon, Ehime, 791-0295, Japan

<sup>e</sup> Department of Analytical Pathology, Ehime University Graduate School of Medicine, Shitsukawa, Toon, Ehime, 791-0295, Japan

<sup>f</sup> Division of Diagnostic Pathology, Ehime University Hospital, Shitsukawa, Toon, Ehime, 791-0295, Japan

## ARTICLE INFORMATION

### Article history:

Received 23 February 2022

Received in revised form

24 June 2022

Accepted 27 June 2022

**AIM:** To evaluate the usefulness of synthetic magnetic resonance imaging (MRI) performed before the initiation of neoadjuvant chemotherapy (NAC) in predicting whether breast cancers can achieve a pathological complete response (pCR) after the completion of NAC.

**MATERIALS AND METHODS:** This retrospective study investigated 37 consecutive patients with 39 breast cancers (pCR: 14, and non-pCR: 25) who underwent dynamic contrast-enhanced (DCE)-MRI and synthetic MRI before the initiation of NAC. Using synthetic MRI images, quantitative values (T1 and T2 relaxation times, proton density [PD] and their standard deviations [SD]) were obtained in breast lesions, before (Pre-T1, Pre-T2, Pre-PD, SD of Pre-T1, SD of Pre-T2, SD of Pre-PD) and after (Gd-T1, Gd-T2, Gd-PD, SD of Gd-T1, SD of Gd-T2, SD of Gd-PD) contrast agent injection. The aforementioned quantitative values and several morphological features that were identified on DCE-MRI were compared between pCR and non-pCR.

**RESULTS:** Multivariate analyses revealed that the SD of Pre-T2 ( $p=0.038$ ) was significant and was an independent predictor of pCR, with an area under the receiver operating characteristics curve of 0.829. The sensitivity, specificity, and accuracy of the SD of Pre-T2 with an optimal cut-off value of 11.5 were 71.4%, 80%, and 76.3%, respectively.

**CONCLUSIONS:** The SD of Pre-T2 obtained from synthetic MRI was used successfully to predict those breast cancers that would achieve a pCR after the completion of NAC; however, these results are preliminary and need to be verified by further studies.

© 2022 The Royal College of Radiologists. Published by Elsevier Ltd. All rights reserved.

\* Guarantor and correspondent: M. Matsuda, Department of Radiology, Ehime University Graduate School of Medicine, Shitsukawa, Toon, Ehime, 791-0295, Japan. Tel.: +81 89-960-5371; fax: +81 89-960-5375.

E-mail address: [megumi@me.ehime-u.ac.jp](mailto:megumi@me.ehime-u.ac.jp) (M. Matsuda).

## Introduction

Breast cancer is a common malignancy, and incidence rates are increasing worldwide.<sup>1</sup> Neoadjuvant chemotherapy (NAC) can decrease tumour volume, which improves the operability of locally advanced breast cancer, reduce metastasis, and detect drug sensitivity; it has been proposed as the standard therapy for locally advanced breast cancer.<sup>2</sup> In patients with operable breast cancer, NAC has been shown to improve breast conservation rates.<sup>3,4</sup> The usual index to evaluate the chemosensitivity of breast cancer is the degree of regression after NAC. A pathological complete response (pCR) is associated with a good prognosis.<sup>2</sup> NAC has several advantages; however, NAC for operable breast cancer is associated with a risk of “under-treatment”—in cases where cancer does not respond to NAC—because NAC generally takes several months to complete. A patient with biologically aggressive cancer may not receive an effective treatment over the course of several months, which increases the risk of tumour metastasis.<sup>2</sup> Therefore, it is important to find a more accurate method to predict tumour response to NAC before treatment.

In patients who plan to receive NAC, pre-treatment breast magnetic resonance imaging (MRI) is widely used because of its high sensitivity in the detection of malignancy and accuracy of clinical staging.<sup>5</sup> Morphological features of dynamic contrast-enhanced (DCE)-MRI, such as enhancement pattern, apparent diffusion coefficient (ADC) values from diffusion-weighted imaging, and quantitative values such as T2 relaxation time have been analysed to predict pCR.<sup>6–10</sup>

Synthetic MRI, a recently developed MRI technique, uses a multi-echo and multi-delay acquisition method for simultaneous measurement of quantitative values such as T1 and T2 relaxation times, and proton-density (PD) image mapping; it can obtain these quantitative values during a single scan. Few previous studies have reported the usefulness of synthetic MRI for determining benign versus malignant breast lesions and for estimating subtypes of breast cancer<sup>11,12</sup>; however, to the authors' knowledge, there have been no previous reports on predicting tumour response to NAC in breast cancer using synthetic MRI. The purpose of this study was to validate the performance of synthetic MRI obtained before the initiation of NAC to predict breast cancers that can achieve a pathological complete response (pCR) after the completion of NAC.

## Materials and methods

### Patient selection

This retrospective study was approved by the institutional review board. Requirement for written informed consent was waived owing to the retrospective study design. Patients who had biopsy-proven primary invasive breast carcinomas who underwent breast MRI, including DCE-MRI and synthetic MRI using 3-T MRI before the initiation of NAC between April 2018 and March 2021 were

enrolled in the study. The following patients were excluded: those who did not undergo breast MRI before NAC and those who underwent breast MRI before NAC, not including synthetic sequences.

### MRI acquisition

Breast MRI examinations were performed using a 3-T MRI system (SIGNA Architect, GE Healthcare, Milwaukee, WI, USA) with an eight-channel, phased-array, breast surface coil with the patient in a prone position.

Axial synthetic MRI acquisition for simultaneous T1, T2, and PD mapping was appended to routine breast MRI sequences, using the multiple-dynamic, multiple-echo (MDME) pulse sequence, also known as Quantification of Relaxation Times and Proton Density by Multiecho acquisition of a saturation-recovery using the Turbo spin-Echo Readout (QRAPMASTER).<sup>13</sup> The MDME sequence was based on two-dimensional (2D) fast spin echo (FSE) with interleaved, section-selective, 120° saturation, and multi-echo acquisition, which provided complex real and imaginary images with two echo times and four automatically calculated saturation delays. Acquired data were then processed to quantify the physical properties of tissues, including T1 and T2 relaxation times, and PD using magnetic resonance image compilation (MAGiC) software, which is a component of the synthetic MRI image processing scanner.

For imaging, the scan time for each synthetic MRI was 233 seconds (total scan time for obtaining synthetic MRI before and after contrast agent injection was 466 seconds), and the MDME sequence was obtained before contrast agent injection and at 12 minutes after injection using the following parameters: 4,470 ms repetition time (TR), 15.5/93.1 ms echo time (TE), 360 × 360 mm field of view (FOV), 256 × 224 matrix, 4 mm section thickness, 0.4 mm interslice gap, 28 sections, echo-train length = 16; and 2.5 acceleration factor.

During conventional MRI examinations, a precontrast diffusion-weighted imaging (DWI) sequence (5,936 ms TR, 66.4 ms TE; reduction factor, 2; number of signals acquired, 8; 128 × 128 matrix size, 36 cm<sup>2</sup> FOV, 4 mm slice thickness, 0.4 mm gap, and 196 seconds scan time) was acquired initially, followed by the unenhanced acquisition of DCE-MRI sequences using a T1-weighted three-dimensional fast spoiled gradient-recalled echo sequence with parallel volume imaging for breast assessment (VIBRANT, GE Healthcare; 7.2 ms TR, 2.4 ms TE, 10° flip angle, 350 × 329 mm FOV, 1.4 mm slice thickness, number of slices, 224, and 350 × 256 acquisition matrix). After an intravenous injection of a 0.2 mmol/kg dose of contrast agent at a rate of 2 ml/s, six post-contrast DCE-MRI sequence scans were acquired starting 60 seconds after injection of the contrast agent at 60-second intervals. The scan time for unenhanced imaging was 60 seconds and for six post-contrast DCE-MRI sequence scans, 360 seconds. Additionally, a T2-weighted fast spin-echo sequence (5,369 ms TR, 85 ms TE, 111° flip angle, 36 cm<sup>2</sup> FOV, 384 × 256 matrix, number of excitations, 2, 4 mm slice thickness, 0.4 mm gap, number of slices, 36, and 183 seconds scan time) was scanned.

## MRI analysis

DCE-MRI findings were retrospectively and individually reviewed and evaluated by 85 two radiologists with 8 (reader 1) and 12 (reader 2) years of experience in breast imaging. For preparation before review and evaluation, two readers confirmed descriptions of morphological features and time–signal intensity curve patterns in the fifth edition of the Breast Imaging Reporting and Data System (BI-RADS).<sup>14</sup> Two readers were given a 15-minute review of some typical morphological features and time–signal intensity curve patterns of the breast lesions. In cases of disagreement, consensual interpretations of morphological characteristics (e.g., shape, spiculate margin, and rim enhancement), time–signal intensity curve patterns,<sup>12,14</sup> and intra-tumoural T2 high signal intensity<sup>15</sup> were obtained. Readers were only provided with lesion locations as detected by mammography and ultrasonography (US) and were blinded to all other information, including the results of conventional mammography, ultrasound (US), and histopathology, as well as any information on clinical radiology reports. Further, both readers independently placed the regions of interest (ROIs) in the highest visual enhancement place within the tumour in the early phase to calculate and assess the contrast enhancement (CE) ratio (CE ratio = [post-contrast signal intensity–pre-contrast signal intensity]/pre-contrast signal intensity) for increased early-phase signal intensities<sup>15,16</sup> and time–signal intensity curve patterns (washout and non-washout). The mean of the CE ratio values were obtained by both readers in the analysis.

Intra-tumoural high signal intensity was defined as that which was stronger than or almost the same as that of water or vessels on fat-suppressed T2-weighted MRI images.<sup>15</sup>

The two readers measured the tumour size independently, with the mean of their measured values being considered the lesion size. The lesion size was determined using its largest diameter in three reformatted planes (i.e., sagittal, axial, and coronal) on DCE-MRI.

The synthetic MRI sequence yielded quantitative maps of T1, T2, and PD, which were then used for measurements to yield synthetic images that matched the conventional images. Each lesion was identified on DCE-MRI, with the lesion location being detected by mammography and US. The two readers drew the ROIs manually on synthetic T2-weighted images to obtain the T1, T2, and PD and standard deviations (SDs) of these quantitative values in breast lesions before and after contrast agent injection. Readers 1 and 2 independently selected a slice and drew the ROIs manually on the synthetic T2-weighted images to include the lesion centres and most of the abnormalities within the lesion borders (Figs 1 and 2). The mean ROI values obtained by both radiologists were included and evaluated as quantitative evaluation values with the synthetic MRI. Values for T1, T2 relaxation time, PD, and SDs of these quantitative values were calculated automatically within the ROI (Pre-T1, Pre-T2, Pre-PD, Gd-T1, Gd-T2, Gd-PD, SD of Pre-T1, SD of Pre-T2, SD of Pre-PD, SD of Gd-T1, SD of Gd-T2, and SD of Gd-PD, respectively).

The ADC was calculated using the following equation:  $ADC = (1/b_2 - b_1) \ln(S_2/S_1)$ . S1 and S2 represented signal intensities in the ROIs obtained using different gradient

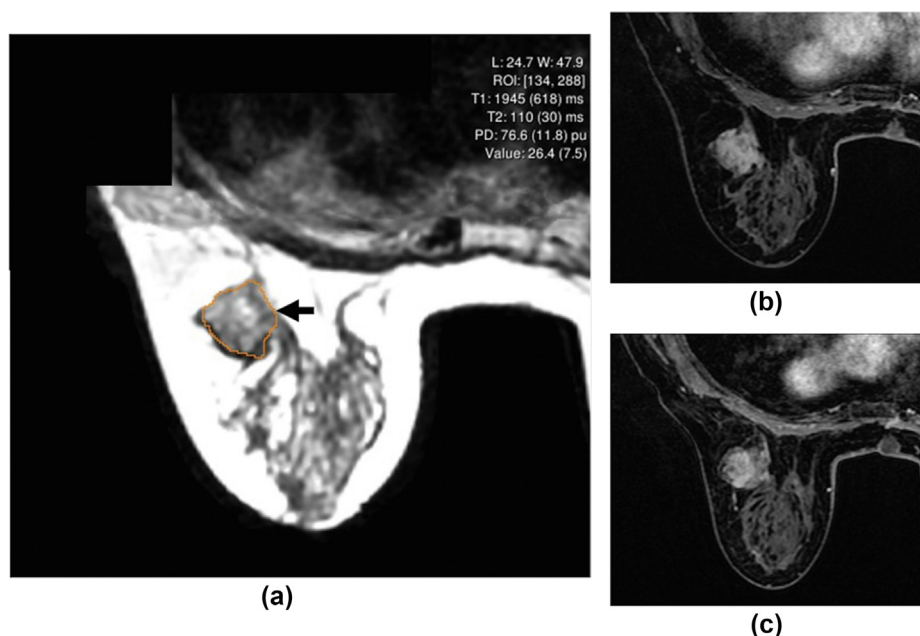


**Figure 1** Images of a 69-year-old woman with triple-negative breast cancer (cT2N1M0 cStage IIB) who had Non-pCR to NAC. (a) Synthetic T2-weighted and (b) DCE-MRI images show an area of enhancement with irregular shape and irregular margin in the right breast before NAC. An ROI delineating the breast lesion was placed in the tumour of the synthetic T2WI (arrow). The contrast-enhancing breast lesion on the DCE-MRI image (b) was delineated manually in the synthetic T2WI. The Pre-T1, Pre-T2, Pre-PD, Pre-T1SD, Pre-T2SD, and Pre-PDSD of the lesion were 1945 ms, 110 ms, 76.6 pu, 618, 30, and 11.8, respectively. The Pre-T2SD of the lesion was 30, which was consistent with non-pCR based on the present results. (c) In DCE-MRI after NAC, residual enhancing mass is visible.

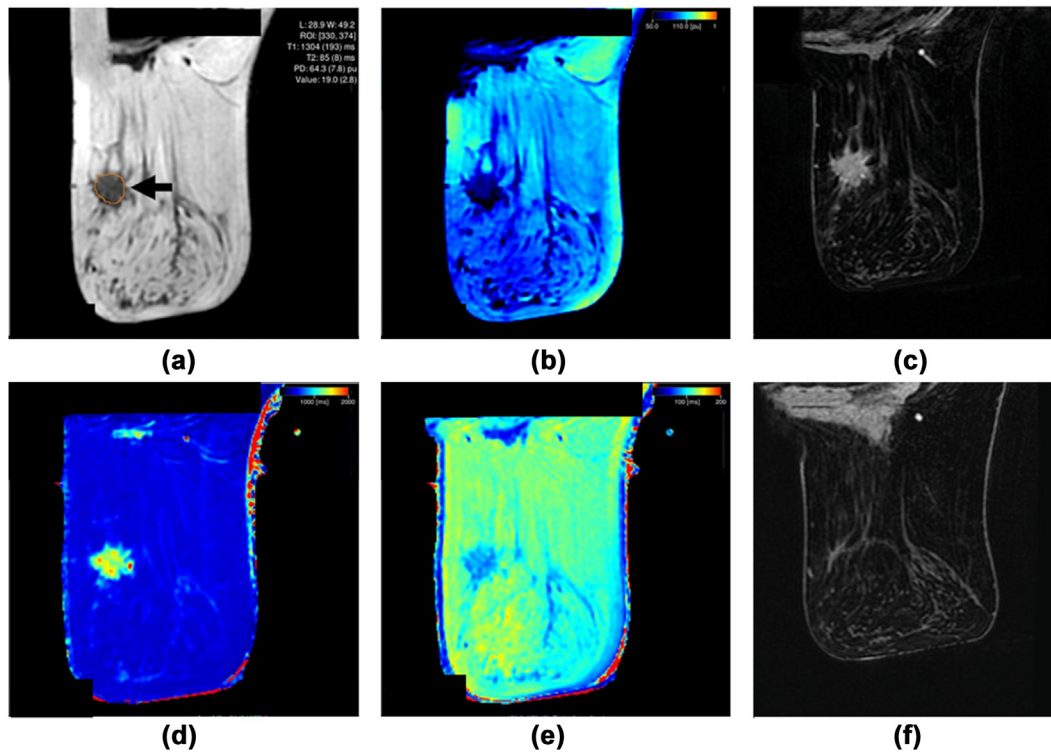


**Figure 2** Images of a 65-year-old woman with Luminal-Her2 breast cancer (cT1cN1M0 cStage IIA) who achieved pCR to NAC. Precontrast (a) T2-weighted image, (b) PD map, (c) T1 map, (d) T2 map Synthetic MRI images and (e) DCE-MRI image show a lobulate mass with irregular shape and spiculate margin in the right breast (arrow) before NAC. The Pre-T1, Pre-T2, Pre-PD, Pre-T1SD, Pre-T2SD, and Pre-PDSD of the lesion were 1304 ms, 85 ms, 64.3 pu, 193, 8, and 7.8, respectively. The Pre-T2SD of the lesion was 8, consistent with pCR based on the present results. (f) On the DCE-MRI image after NAC, an area of subtle enhancement is visible.

factors  $b_1$  and  $b_2$  ( $b$ -values of 0 and  $1000 \text{ s/mm}^2$ , respectively).<sup>17</sup> For ADC value measurements, the two readers drew the ROIs manually and independently, and their mean values were analysed as ADC values. The ROIs of breast lesions were drawn manually to include most abnormalities within the breast lesion borders, as was done in the synthetic image generation. The ADC value was measured automatically by drawing the ROI. Additionally, the electronic medical record database was searched to identify each patient's age at diagnosis and chemotherapy regimen.

#### Pathological assessment

Tumour features were obtained from histopathological reports of core-needle biopsies performed prior to NAC. The analysis was performed independently by two pathologists. When disagreements occurred, a consensus was reached through discussion. Streptavidin–peroxidase immunohistochemistry (IHC) was used to determine the oestrogen receptor (ER), progesterone receptor (PgR), HER2, and Ki-67 expression levels in each patient. ER and PgR positivity were defined as the presence of  $\geq 1\%$  positively stained nuclei in 10 high-power fields.<sup>18</sup> ER and/or PgR positivity was considered hormone receptor (HR)-positive, while both ER and PgR negativity were considered HR-negative. HER2 positivity was defined as an IHC HER2 score of 3 or as gene

amplification observed by fluorescence in-situ hybridisation in tumours with an IHC HER2 score  $\geq 2$ . Tumour subtypes were classified as follows:

- (i) *luminal A*: HR-positive, HER2-negative, and Ki-67 low ( $\leq 14\%$ );
- (ii) *luminal B*: HR-positive, HER-2-negative and Ki-67 high ( $>14\%$ ); (iii) *luminal-HER2*: HR-positive, HER2-positive and any Ki-67 level; (iv) *HER2-enriched*: HR-negative and HER2-positive; and (v) *triple-negative breast cancers (TNBCs)*: HR-negative and HER2-negative.<sup>19,20</sup>

The histological response to NAC was evaluated by a histopathological examination of the final surgical specimen after the completion of NAC. The General Rules for Clinical and Pathological Recording of Breast Cancer, version 18 (2018), edited by the Japanese Breast Cancer Society, was used to define pCR.<sup>21</sup> The effect on invasive lesions was evaluated microscopically. Grade 0: little change, grade 1a: mild effect, grade 1b: moderate effect, grade 2a: marked effect but with viable cancer cells, grade 2b: significant effect with only a few viable cancer cells, and grade 3: no viable cancer cells seen (pCR). In this guideline, pCR is defined as the complete absence of invasive lesions, regardless of the presence of ductal carcinoma in situ (DCIS).

## Statistical analysis

Statistical analyses were performed using SPSS (version 26.0, Chicago, IL, USA) with statistical significance set at  $p < 0.05$ . Continuous measures are summarised as means and standard deviations. Ages, lesion sizes, values and SDs of longitudinal T1 values, transverse T2 relaxation times, PD, CE ratios, and ADC values of the patients were compared between pCR and non-pCR using the Mann–Whitney *U*-test. Morphological features, time–signal intensity curve patterns, and intra-tumoural high signal intensity on fat-suppressed T2-weighted MRI images of the lesions were analysed using Fisher's exact test. The variables indicated as significant in the univariate analysis were further analysed using multivariate analysis (binominal logistic regression analysis). The cut off *p*-value used to build the multivariate model was 0.05. The effectiveness of SD of Pre-T2 in differentiating between pCR and non-pCR was evaluated using receiver operating characteristic (ROC) analysis. The optimal threshold for distinguishing between pCR and non-pCR was determined through identification of the highest possible sensitivity and specificity (maximal Youden index defined as sensitivity + specificity – 1) on the ROC curves. The area under the ROC curve (AUC) is presented as the mean and 95% confidence interval (CI). Interobserver agreement was assessed via kappa values for qualitative data (time signal intensity pattern, shape, spiculate margin, rim enhancement, and intra-tumoural T2 high signal intensity) and intraclass correlation coefficient (ICC) for quantitative data (quantitative values acquired using

synthetic MRI, CE ratio, ADC value, and lesion size). Kappa values were interpreted as follows: excellent, 0.81–1.00; good, 0.61–0.80; moderate, 0.41–0.60; fair, 0.21–0.40; and poor,  $\leq 0.20$ . ICCs were interpreted as follows: excellent, 0.75–1.00; good, 0.60–0.74; fair, 0.41–0.59; and poor,  $\leq 0.40$ .<sup>22</sup>

## Results

During the recruitment period, 64 patients with invasive breast cancer received NAC. One patient, whose breast MRI was not performed before NAC, was excluded. The remaining 63 patients underwent MRI before NAC. Of 63 patients, 26 patients scanned with breast MRI before NAC, not including synthetic sequences, were excluded from the analysis. Of excluded 26 patients, 10 patients were scanned using 1.5 T MRI, 13 patients were scanned using 3 T MRI without additional synthetic sequences, and three patients MRI were scanned at another institution. Finally, a total of 37 patients (age: 30–77 years; mean: 54 years) with 39 invasive breast carcinomas who underwent DCE-MRI and synthetic MRI with 3-T MRI before the initiation of NAC between April 2018 and March 2021 were included in the study. The molecular subtypes of invasive breast carcinomas were as follows: luminal A ( $n=2$ , 5.1%), luminal B ( $n=9$ , 23.1%), luminal-HER2 ( $n=8$ , 20.5%), HER2-enriched ( $n=6$ , 15.4%), and triple-negative ( $n=14$ , 35.9%).

Of the 39 included lesions, 25 (lesion size: mean  $\pm$  SD, 30.82  $\pm$  13.79; range, 8.5–53) showed non-pCR and 14 (lesion size: mean  $\pm$  SD, 36.04  $\pm$  14.82; range, 13.5–73.5)

**Table 1**

Comparison of the quantitative values and image findings of all 39 breast cancers acquired using synthetic MRI and DCE-MRI (non-pCR versus pCR).

	Non-pCR (n=25)	pCR (n=14)	<i>p</i> -Value <sup>a</sup>	<i>p</i> -Value <sup>b</sup>
Quantitative values acquired using synthetic MRI				
Pre-T1 (ms)	1320.59 $\pm$ 435.34	1401.54 $\pm$ 280.78	0.703	
Pre-T2 (ms)	86.74 $\pm$ 12.15	93.29 $\pm$ 17.73	0.629	
Pre-PD	78.24 $\pm$ 11.68	77.59 $\pm$ 6.98	0.815	
SD of Pre-T1	221.76 $\pm$ 99.77	149.18 $\pm$ 39.04	0.006 <sup>c</sup>	0.059
SD of Pre-T2	16.24 $\pm$ 7.32	9.64 $\pm$ 3.18	0.001 <sup>c</sup>	0.038 <sup>c</sup>
SD of Pre-PD	4.62 $\pm$ 2.25	3.74 $\pm$ 1.38	0.169	
Gd-T1 (ms)	662.22 $\pm$ 185.02	634.07 $\pm$ 78.41	0.747	
Gd-T2 (ms)	76.65 $\pm$ 11.57	82.21 $\pm$ 12.98	0.412	
Gd-PD	83.30 $\pm$ 12.07	82.85 $\pm$ 8.15	0.849	
SD of Gd-T1	82.17 $\pm$ 52.92	50.14 $\pm$ 11.97	0.011 <sup>c</sup>	0.169
SD of Gd-T2	6.35 $\pm$ 2.52	5.14 $\pm$ 2.34	0.051	
SD of Gd-PD	4.21 $\pm$ 1.93	4.35 $\pm$ 3.62	0.359	
Quantitative values and image findings acquired using DCE-MRI				
ADC value ( $\times 10^3$ mm/s) (mean $\pm$ SD)	959.31 $\pm$ 251.07	953.27 $\pm$ 175.41	0.725	
CE ratio	1.31 $\pm$ 0.33	1.59 $\pm$ 0.57	0.139	
Time–signal intensity curve pattern (washout/non-washout)	9(36)/16(64)	10(29)/4(71)	0.048 <sup>c</sup>	0.078
Shape (round or oval/irregular)	3(12)/22(88)	5(36)/9(64)	0.109	
Spiculate margin (+/–)	7(28)/18(72)	3(21)/11(79)	0.721	
Rim enhancement (+/–)	8(32)/17(68)	7(50)/7(50)	0.318	
Intra-tumoural T2 high signal intensity (+/–)	9(36)/16(64)	5(36)/9(94)	1.00	
Lesion size (mm)	36.04 $\pm$ 14.82	30.82 $\pm$ 13.79	0.437	

Values in bold are the number of lesions with percentages in parentheses.

DCE-MRI, dynamic contrast-enhanced magnetic resonance imaging; pCR, pathological complete response; PD, proton density; ADC, apparent diffusion coefficient; SD, standard deviation; CE ratio, contrast enhancement ratio.

<sup>a</sup> Univariate analysis.

<sup>b</sup> Multivariate analysis.

<sup>c</sup>  $p < 0.05$ , results are statistically significant.

**Table 2**  
Clinical characteristics and histological types.

	Non-pCR (n=25)	pCR (n=14)	p-Value <sup>a</sup>
Age at diagnosis (years) (mean; range)	55, 30–77	52, 31–67	0.814
T (1/2/3/4)	2/13/5/5	5/8/0/1	
N (0/1/2/3)	8/14/0/3	3/8/1/2	
M (0/1)	25/0	14/0	
Stage (I/II/III/IV)	2/15/8/0	2/8/4/0	
Type of surgery (total mastectomy/conservative surgery)	16/9	10/4	
Histological type	NST 24 Mucinous carcinoma 1	NST 12 Squamous cell carcinoma 1 Apocrine carcinoma 1	
Chemotherapy regimens by subtypes			
Triple negative	10	4	
AC→DTX	6	3	
AC→PTX	4	1	
Luminal A-like	2	0	
ddAC→wPTX	2	0	
Luminal B-like	7	2	
AC→DTX	4	0	
ddAC→wPTX	0	1	
ddAC→wPTX + HER + PER	1	0	
ddAC→PTX	1	1	
AC→DTX + HER	1	0	
Luminal-HER2	4	4	
AC→PER + HER + DTX	1	1	
AC→DTX + HER	1	0	
AC→HPD	1	1	
AC→TX + HER	0	1	
ddAC→PER + HER + DTX	1	0	
AC→DTX	0	1	
HER2-enriched	2	4	
AC→DTX + HER + PER	0	4	
ddAC→wPTX + HER + PER	1	0	
AC→DTX + HER	1	0	

pCR, pathological complete response; NST, no special type; AC, adriamycin; cyclophosphamide; DTX, docetaxel; PTX, paclitaxel; ddAC, dose-dense AC; wPTX, weekly paclitaxel; HER, trastuzumab; PER, pertuzumab.

<sup>a</sup> Univariate analysis.

showed pCR. Histopathological diagnoses were confirmed in all 39 lesions, with specimens obtained from core-needle biopsy before the initiation of NAC. Stratified by tumour subtypes, pCR was observed in 0% (0/2) of luminal A, 22.2% (2/9) of luminal B, 50% (4/8) of luminal-HER2, 66.7% (4/6) of HER2-enriched, and 28.6% (4/14) of TNBCs. Fig. 2 shows a representative case of pCR.

The MRI examinations were performed before or at least 2 weeks after biopsy to avoid artefacts.<sup>23</sup> Table 1 shows the quantitative values and image findings obtained from synthetic MRI and DCE-MRI and Table 2 shows the clinical characteristics, chemotherapy regimens, and histological types of included cases. Univariate analysis revealed that the SD of Gd-T1 ( $p=0.011$ ), SD of Pre-T1 ( $p=0.006$ ), and SD of Pre-T2 ( $p=0.001$ ) were significantly higher in non-pCR than in pCR based on the quantitative values obtained from the synthetic MRI. MRI findings showed that the washout curve pattern was observed significantly more commonly in pCR than in non-pCR ( $p=0.048$ ). Other quantitative values and image findings obtained from synthetic MRI and DCE-MRI were not significantly different between non-pCR and pCR (Table 1). Further, multivariate analysis showed that SD of Pre-T2 ( $p=0.038$ ) was a significant predictor for differentiating between non-pCR and pCR.

The univariate and multivariate analysis results for pCR and non-pCR are shown in Table 1. ROC analysis revealed AUCs of 0.829 for SD of Pre-T2 (95% CI, 0.700–0.957), with an optimal SD of Pre-T2 cut-off value of 11.50 for differentiating between non-pCR and pCR (Fig 3). The diagnostic performance of several potential methods for differentiating these groups was evaluated, including the use of SD of Pre-T2 with the aforementioned optimal cut-off value. The sensitivity, specificity, positive predictive value, negative predictive value, and accuracy of the SD of T2-Pre with an optimal cut off value of 11.5 were 71.4% (95% IC: 47.8–95.1), 80% (95% IC: 64.3–95.7), 66.7% (95% IC: 42.8–90.5), 83.3% (95% IC: 68.4–98.2), and 76.3% (95% IC: 63.7–90.1), respectively. Interobserver agreements of quantitative and qualitative data were satisfactory (ICC: 0.82–0.97, kappa value: 0.79–0.90; Table 3).

## Discussion

The results of this study demonstrate that the SD of Pre-T2 was useful in predicting breast cancers that could achieve a pCR after the completion of NAC. There have been few published reports about quantitative values of the breast

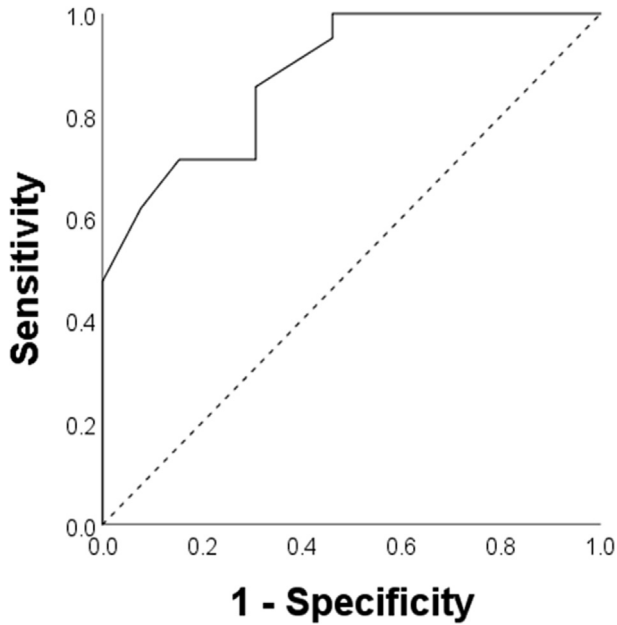


**Figure 3** ROC curve of SD of Pre-T2 in differentiating breast cancers achieving pCR from non-pCR in response to NAC. The diagonal line represents an AUC of 0.50.

lesions obtained from synthetic MRI, including not only T1, T2, and PD, but also SD of these quantitative values.<sup>24</sup> Similarly, the present study evaluated SDs, which is a strength of this study. The T2 value of the tumour is

**Table 3**  
Interobserver agreements between two readers for quantitative and qualitative data.

Quantitative data		
	ICCs	95%CI
Pre-T1	0.944	0.896–0.970
Pre-T2	0.882	0.787–0.937
Pre-PD	0.933	0.877–0.964
SD of Pre-T1	0.822	0.688–0.903
SD of Pre-T2	0.831	0.625–0.918
SD of Pre-PD	0.969	0.942–0.984
Gd-T1	0.866	0.760–0.927
Gd-T2	0.857	0.744–0.923
Gd-PD	0.878	0.781–0.934
SD of Gd-T1	0.901	0.812–0.948
SD of Gd-T2	0.856	0.743–0.921
SD of Gd-PD	0.844	0.724–0.915
ADC value	0.895	0.808–0.943
CE ratio	0.860	0.750–0.924
Lesion size	0.941	0.891–0.969
		Kappa values
Time–signal intensity curve pattern		0.897
Shape		0.793
Spiculate margin		0.874
Rim enhancement		0.835
Intra-tumoural T2 high signal intensity		0.825

Agreement according to Kappa value was 0.81–1.00, excellent; 0.61–0.80, good; 0.41–0.60, moderate; 0.21–0.40, fair; and ≤0.20, poor.

Agreement according to ICC was 0.75–1.00, excellent; 0.60–0.74, good; 0.41–0.59, fair; and ≤0.40, poor.

ICC, intraclass correlation coefficient; CI, confidence interval; PD, proton density; SD, standard deviation; ADC, apparent diffusion coefficient; CE ratio, contrast enhancement ratio.

associated with intra-tumoural necrosis and hypoxia; previous studies have reported their association with the effect of neoadjuvant chemotherapy on breast cancers.<sup>15,25,26</sup> Necrosis within the tumour is likely to be poorly perfused, which reduces the delivery of chemotherapeutic agents to the tumour. Furthermore, hypoxia cancer cells near the necrotic area are more likely to have a slow metabolism and, therefore, are less sensitive to chemotherapy.<sup>27</sup> In the present study, the SD of Pre-T2 obtained from synthetic MRI was significantly higher in non-pCR ( $16.24 \pm 7.32$ ) than in pCR ( $9.64 \pm 3.18$ ). High Pre-T2 SD leads to tumour heterogeneity owing to tumour necrosis; however, detailed pathological verification was not performed.

Previous studies have investigated the relationships between pre-treatment DCE-MRI findings and pCR in breast cancer. In these studies, the washout pattern in the delayed phase on DCE-MRI was identified as a predictive factor for pCR.<sup>28,29</sup> In addition, Park *et al.* reported that ADC values on pre-treatment MRI were significantly lower in responders than in non-responders.<sup>26</sup> Although not significant in the multivariate analysis, the present study also demonstrated that the washout pattern in the delayed phase on DCE-MRI was observed significantly more commonly in pCR (washout/non-washout: 10/4) than in non-pCR (washout/non-washout: 9/16;  $p=0.078$ ). There were no significant differences in ADC values and shapes between pCR and non-pCR. The difference in the results may be attributed to differences in patient populations (number of enrolled patients, subtypes, and histological breast cancer types).

Furthermore, previous studies have explored the relationship between intrinsic subtypes of breast cancer and response to NAC. The luminal A breast cancer corresponds to low-proliferating tumours with an excellent prognosis factor, whereas the triple-negative breast cancer represents the most biologically aggressive subtype of breast cancer. Paradoxically, a complete response is almost never observed in the luminal A breast cancer; however, a complete response can be expected in one-third of the triple-negative breast cancers.<sup>30,31</sup> Santamaria *et al.* conducted a study to investigate if pCR could be predicted from pre-treatment MRI images in various subtypes of breast cancer.<sup>32</sup> They excluded luminal A breast cancers because these tumours did not respond to NAC and pCR was not expected in their patient collective. In the present study, all enrolled luminal A breast cancers were not pCR; however, the main goal of the study was to evaluate the utility of synthetic MRI obtained before NAC in predicting breast cancer achieving a pCR after the completion of NAC, and to identify which quantitative values calculated using synthetic MRI would be most useful for predicting pCR in various breast cancer subtype. Therefore, luminal A breast cancers were also included in the enrolled lesions. Previous studies on the utility of MRI for assessing response to ongoing or completed NAC have demonstrated that the prediction of achievement of a pCR state may vary with tumour subtypes.<sup>2,32</sup> Therefore, specific predictors of pCR should be considered for each breast cancer subtype.

This study has several limitations. First, and most importantly, this was a preliminary retrospective single-

institution study with a small sample size. Analysing many parameters, despite the small sample size, may be prone to inherent bias. Using both quantitative values obtained from synthetic MRI and image findings of DCE-MRI scanned before the initiation of NAC may improve the accuracy of prediction of achievement of a pCR state; however, the sample size and composition may affect results, including optimal SD of Pre-T2 cut-off value. Therefore, further multicentre, large-scale studies are needed to reveal how useful synthetic MRI is to predict the achievement of a pCR state, and improve the generalisability and applicability of the present results in clinical practice. Second, 26 patients were excluded from the analysis based on the exclusion criteria, causing a potential selection bias. Third, NAC regimens were not unified for each histological subtype of breast cancer. The selection of the NAC regimen has been suggested to influence the pCR rate. Additional studies that include more cases with a unified NAC regimen for each subtype are needed. Fourth, the quantitative synthetic MRI values for the whole tumour were not measured, and therefore, the values were not necessarily representative of the whole tumour; however, few previous studies that obtained quantitative values of breast cancers using synthetic MRI<sup>11,24</sup> had values that were similar to the present study. Fifth, the enrolled lesions included special types of breast cancer (one mucinous carcinoma, one squamous cell carcinoma, and one apocrine carcinoma). These lesions may affect quantitative values obtained from synthetic MRI and image findings of DCE-MRI; however, all histological types of breast cancer, including special and non-special types, may also receive NAC. Moreover, the study evaluated the utility of synthetic MRI before NAC for predicting pCR in various breast cancers. Therefore, special types of breast cancer were also included in the enrolled lesions. Finally, the added MDME sequence for the acquisition of synthetic MRI increases the scan time. It is desirable to optimise the technology to shorten the scan time.

In conclusion, this study demonstrated that the quantitative values of synthetic MRI, especially SD of Pre-T2, may be useful for predicting whether breast cancers can achieve a pCR after the completion of NAC.

## Declaration of competing interest

The authors declare no conflict of interest.

## References

- Bray F, Jemal A, Grey N, et al. Global cancer transitions according to the Human Development Index (2008–2030): a population-based study. *Lancet Oncol* 2012;**13**:790–801. [https://doi.org/10.1016/S1470-2045\(12\)70211-5](https://doi.org/10.1016/S1470-2045(12)70211-5).
- Tsukada H, Tsukada J, Schrading S, et al. Accuracy of multi-parametric breast MR imaging for predicting pathological complete response of operable breast cancer prior to neoadjuvant systemic therapy. *Magn Reson Imag* 2019;**62**:242–8. <https://doi.org/10.1016/j.mri.2019.07.008>.
- Fisher B, Brown A, Mamounas E, et al. Effect of preoperative chemotherapy on local regional disease in women with operable breast cancer: findings from National Surgical Adjuvant Breast and Bowel Project B-18. *J Clin Oncol* 1997;**15**:2483–93. <https://doi.org/10.1200/JCO.1997.15.7.2483>.
- Gralow JR, Burstein HJ, Wood W, et al. Preoperative therapy in invasive breast cancer: pathologic assessment and systemic therapy issues in operable disease. *J Clin Oncol* 2008;**26**:814–9. <https://doi.org/10.1200/JCO.2007.15.3510>.
- Yeh E, Slanetz P, Kopans DB, et al. Prospective comparison of mammography, sonography, and MRI in patients undergoing neo-adjuvant chemotherapy for palpable breast cancer. *AJR Am J Roentgenol* 2005;**184**:868–77. <https://doi.org/10.2214/ajr.184.3.01840868>.
- Drisis S, Metens T, Ignatiadis M, et al. Quantitative DCE-MRI for prediction of pathological complete response following neoadjuvant treatment for locally advanced breast cancer: the impact of breast cancer subtypes on the diagnostic accuracy. *Eur Radiol* 2016;**26**:1474–84. <https://doi.org/10.1007/s00330-015-3948-0>.
- O'Flynn EA, Collins D, D'Arcy J, et al. Multi-parametric MRI in the early prediction of response to neo-adjuvant chemotherapy in breast cancer: value of non-modelled parameters. *Eur J Radiol* 2016;**85**:837–42. <https://doi.org/10.1016/j.ejrad.2016.02.006>.
- Eom HJ, Cha JH, Choi WJ, et al. Predictive clinicopathologic and dynamic contrast-enhanced MRI findings for tumour response to neoadjuvant chemotherapy in triple-negative breast cancer. *AJR Am J Roentgenol* 2017;**208**:W225–30. <https://doi.org/10.2214/AJR.16.17125>.
- Li X, Abramson RG, Arlinghaus LR, et al. Multiparametric magnetic resonance imaging for predicting pathological response after the first cycle of neoadjuvant chemotherapy in breast cancer. *Invest Radiol* 2015;**50**:195–204. <https://doi.org/10.1097/RLI.000000000000100>.
- Liu L, Yin B, Geng DY, et al. Change of T2 relaxation time from neo-adjuvant chemotherapy in breast cancer lesions. *Iran J Radiol* 2016;**13**:e24014. <https://doi.org/10.5812/iranjrad.24014>.
- Du S, Gao S, Zhang L, et al. Improved discrimination of molecular subtypes in invasive breast cancer: comparison of multiple quantitative parameters from breast MRI. *Magn Reson Imag* 2021;**77**:148–58. <https://doi.org/10.1016/j.mri.2020.12.001>.
- Matsuda M, Tsuda T, Ebihara R, et al. Enhanced masses on contrast-enhanced breast: differentiation using a combination of dynamic contrast-enhanced MRI and quantitative evaluation with synthetic MRI. *J Magn Reson Imag* 2021;**53**:381–91. <https://doi.org/10.1002/jmri.27362>.
- Wartnjes JB, Dahlqvist O, Lundberg P. Novel method for rapid, simultaneous T1, T2\*, and proton density quantification. *Magn Reson Med* 2007;**57**:528–37. <https://doi.org/10.1002/mrm.21165>.
- D'Orsi CJ, Sickles EA, Mendelson EB, et al. *ACR BI-RADS Atlas, breast imaging reporting and data system*. Reston, VA: American College of Radiology; 2013.
- Uematsu T, Kasami M, Yuen S. Triple-negative breast cancer: correlation between MR imaging and pathologic findings. *Radiology* 2009;**250**:638–47. <https://doi.org/10.1148/radiol.2503081054>.
- Kuhl CK, Mielcareck P, Klaschik S, et al. Dynamic breast MR imaging: are signal intensity time course data useful for differential diagnosis of enhancing lesions? *Radiology* 1999;**211**:101–10. <https://doi.org/10.1148/radiology.211.1.r99ap38101>.
- Kim KW, Kuzmiak CM, Kim YJ, et al. Diagnostic usefulness of combination of diffusion-weighted imaging and T2WI, including apparent diffusion coefficient in breast lesions: assessment of histologic grade. *Acad Radiol* 2018;**25**:643–52. <https://doi.org/10.1016/j.acra.2017.11.011>.
- Hammond ME, Hayes DF, Wolff AC, et al. American Society of Clinical Oncology/College of American Pathologists guideline recommendations for immunohistochemical testing of estrogen and progesterone receptors in breast cancer. *J Oncol Pract* 2010;**6**:195–7. <https://doi.org/10.1200/JOP.777003>.
- Hammond MEH, Hayes DF, Dowsett M, et al. American Society of Clinical Oncology/College of American Pathologists guideline recommendations for immunohistochemical testing of estrogen and progesterone receptors in breast cancer. *J Clin Oncol* 2010;**28**:2784–95. <https://doi.org/10.1200/JCO.2009.25.6529>.
- Wolff AC, Hammond MEH, Allison KH, et al. Human epidermal growth factor receptor 2 testing in breast cancer: American Society of Clinical Oncology/College of American Pathologists clinical practice guideline focused update. *J Clin Oncol* 2018;**36**:2105–22. <https://doi.org/10.1200/JCO.2018.77.8738>.

21. The Japanese Breast Cancer Society. *The general rules for clinical and pathological recording of breast cancer*. 18th edition. Tokyo: Kanehara Shuppan; 2018 (in Japanese).
22. Cicchetti DV. Guidelines, criteria, and rules of thumb for evaluating normed and standardized assessment instruments in psychology. *Psychol Assess* 1994;**6**:284–90. <https://doi.org/10.1037/1040-3590.6.4.284>.
23. Seo M, Ryu JK, Jahng GH, et al. Estimation of T2\* relaxation time of breast cancer: correlation with clinical, imaging and pathological features. *Korean J Radiol* 2017;**18**:238–48. <https://doi.org/10.3348/kjr.2017.18.1.238>.
24. Matsuda M, Kido T, Tsuda T, et al. Utility of synthetic MRI in predicting the Ki-67 status of oestrogen receptor-positive breast cancer: a feasibility study. *Clin Radiol* 2020;**75**:398.e1–8. <https://doi.org/10.1016/j.crad.2019.12.021>.
25. Tan PC, Pickles MD, Lowry M, et al. Lesion T2 relaxation times and volumes predict the response of malignant breast lesions to neoadjuvant chemotherapy. *Magn Reson Imag* 2008;**26**:26–34. <https://doi.org/10.1016/j.mri.2007.04.002>.
26. Park SH, Moon WK, Cho N, et al. Diffusion-weighted MR imaging: pre-treatment prediction of response to neoadjuvant chemotherapy in patients with breast cancer. *Radiology* 2010;**257**:56–63. <https://doi.org/10.1148/radiol.10092021>.
27. Humphries PD, Sebire NJ, Siegel MJ, et al. Tumours in pediatric patients at diffusion-weighted MR imaging: apparent diffusion coefficient and tumour cellularity. *Radiology* 2007;**245**:848–54. <https://doi.org/10.1148/radiol.2452061535>.
28. Tsunoda-Shimizu H, Hayashi N, Hamaoka T, et al. Determining the morphological features of breast cancer and predicting the effects of neoadjuvant chemotherapy via diagnostic breast imaging. *Breast Cancer* 2008;**15**:133–40. <https://doi.org/10.1007/s12282-008-0030-7>.
29. Craciunescu OI, Blackwell KL, Jones EL, et al. DCE-MRI parameters have potential to predict response of locally advanced breast cancer patients to neoadjuvant chemotherapy and hyperthermia: pilot study. *Int J Hyperthermia* 2009;**25**:405–15. <https://doi.org/10.1080/02656730903022700>.
30. Goldhirsch A, Wood WC, Coates AS, et al. Strategies for subtypes—dealing with the diversity of breast cancer: highlights of the St. Gallen international expert consensus on the primary therapy of early breast cancer 2011. *Ann Oncol* 2011;**22**:1736–47. <https://doi.org/10.1093/annonc/mdr304>.
31. Huober J, von Minckwitz G, Denkert C, et al. Effect of neoadjuvant anthracycline–taxane-based chemotherapy in different biological breast cancer phenotypes: overall results from the GeparTrio study. *Breast Cancer Res Treat* 2010;**124**:133–40. <https://doi.org/10.1007/s10549-010-1103-9>.
32. Santamaría G, Bargalló X, Ganau S, et al. Multiparametric MR imaging to assess response following neoadjuvant systemic treatment in various breast cancer subtypes: comparison between different definitions of pathologic complete response. *Eur J Radiol* 2019;**117**:132–9. <https://doi.org/10.1016/j.ejrad.2019.06.009>.